Functional Materials 16, No.4 (2009) 

# Structure features and paramagnetic centres in oxide nanopowders

*V.N.Shevchuk, D.I.Popovych*[*], *Yu.N.Usatenko*[**], *P.Yu.Demchenko*[***], *R.Ya.Serkiz*[**]

Department of Electronics, I.Franko Lviv National University, 50 Drahomanova St., 79005 Lviv, Ukraine
[*]Ya.Pidstryhach Institute of Applied Problems of Mechanics and Mathematics, National Academy of Sciences of Ukraine, 3b Naukova St., 79060 Lviv, Ukraine
[**]Scientific and Technical Center of Low-Temperature Investigations, Ivan I.Franko Lviv National University, 50 Drahomanova St., 79005 Lviv, Ukraine
[***]Interdepartment Scientific and Educational Laboratory of X-ray Structure Analysis, I.Franko Lviv National University, 8 Kyryla and Mefodiya St., 79005 Lviv, Ukraine

*Received April 22, 2009*

Nanopowders ZnO, $SiO_2$, $SiO_2$/10 % $V_2O_5$ obtained by sol-gel technology were investigated by electron paramagnetic resonance (EPR) method at temperature of liquid nitrogen. The structures of the samples are analyzed by X-ray diffraction method. Surface morphology and chemical elementwise composition of powders were studied using scanning electron microscopy. For the nanocomposite $SiO_2$/10 % $V_2O_5$ structure of EPR spectrum is described as a result of unpaired electron and isotope nucleus $^{51}V$ interaction. The prevailed EPR signal in ZnO is hypothetically associated with single-charge vacancy in oxygen sub-lattice.

Нанопорошки ZnO, $SiO_2$, $SiO_2$/10% $V_2O_5$, полученные по sol-gel-технологии, исследованы методом электронного парамагнитного резонанса (ЭПР) при температуре жидкого азота. Структура образцов проанализирована с использованием методарентгеновской дифракции. Морфология поверхности и химический элементный состав порошков изучался сканирующим электронным микроскопом. Для нанокомпозита $SiO_2$/10 % $V_2O_5$ структура ЭПР спектра приписывается результату взаимодействия неспаренного электрона с ядром изотопа $^{51}V$. Доминирующий сигнал ЭПР в ZnO предварительно связывается с однозарядной вакансией в кислородной подрешетке.

In modern nanotechnologies, the oxide powders are among basic materials. Silicon dioxide $SiO_2$ is traditionally used in medical chemistry [1] and nanoelectronics [2]. This compound is also widely used as modifier of properties of other nanomaterials [3]. Thus, nanocomposite ZnO-high-dispersed $SiO_2$ shows 10–50 times more intensive photoluminescence in comparison to nano-ZnO [4], which is used in luminescent gas sensors [5]. Introduction of nanoscale $SiO_2$ into polymers causes considerable modification of their supermolecular structure [6], and such dopants contribute to high conduction properties of proton conductors [7]. Surface $SiO_2$ thin layer on magnetite elevates its thermal stability [8].

The technical characteristics of $SiO_2$ powder can be improved by introducing vanadium nanoclusters [9]. In synthesis of

nanocomposite $SiO_2/V_2O_5$ at certain atomic ratio V/Si, an important role belongs to formation of vanadium pentaoxide microcrystals. Nanocomposite $SiO_2/V_2O_5$ is known also as a catalyst system [10–12].

Practical usefulness of nanomaterials as thermodynamically non-equilibrium systems [13] substantially depends on their defects. Thus, properties of nanomaterials, size effects, stability and reproducibility of characteristics depend upon their structure point defects. The electron paramagnetic resonance (EPR) method is an informative and sensitive instrument for the study of nanomaterials [14]. By this method, ZnO nanopowders were investigated under high pressures [15]. EPR signals were detected also in $ZrO_2$ — pure and doped by transition ions [16, 17]. For nanopowders,the vacancy-type structural defects are predominant and cause the EPR signals.

The elementary defects of $SiO_2$ and $V_2O_5$ were investigated by different methods, including the EPR technique (see e.g. [18–21] and [22, 23], respectively). Features of catalytic active centers in nanocomposite $SiO_2/V_2O_5$ were investigated by EPR method. The investigated samples of different structure and morphology of the starting oxides and final compounds [24–26] were obtained by different methods. In [24] $SiO_2/V_2O_5$ nanocomposite was obtained by a five-fold incipient wetness impregnation/drying with a final calcination on air. Also, $SiO_2/V_2O_5$ was synthesized by ion exchange method in a film form with subsequent drying at room temperature for two days [25]. In [26], the nanocomposite was obtained by flame pyrolysis with different $SiO_2/V_2O_5$ ratios and values of surface areas (40–80 $m^2/g$). However, the features of the obtained structure and the nature of point defects and paramagnetic centres in nanomaterials have not been established reliably.

In this work, ZnO, $SiO_2$ and $SiO_2/V_2O_5$ composite nanopowders were studied by EPR method. The characterization of the nanopowders was carried out using X-ray diffraction (XRD) patterns.

ZnO, $SiO_2$ and $SiO_2/10\ \%V_2O_5$ composite nanopowders were obtained by liquid-phase method of sol-gel technology [27]. At the final stage, the synthesized materials in each individual case were stirred, washed and dried up to the forming of fine powders. The surface morphology of the samples was studied using a REMMA-102-02 type scanning electron microscope (SELMI, Ukraine) [28].

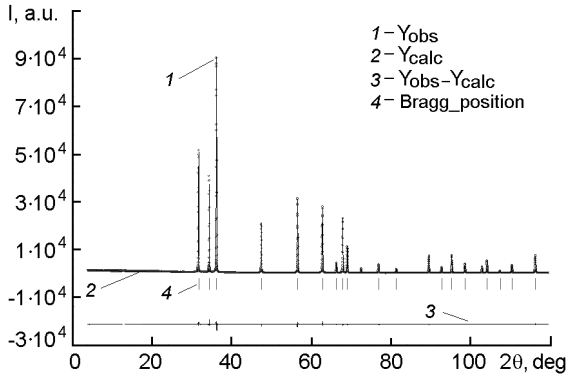


Fig. 1. X-ray diffraction data for ZnO.

XRD analysis was performed using a STOE STADI P Powder Diffraction System. The arrays of experimental intensities and reflection angles from the investigated patterns were obtained using the above mentioned diffractometer with a linear positional sensitive detector PSD upon modified Ghinier geometry scheme, with Bragg-Brentano modes for transmission. Conditions of the measurements: pure CuKα1 radiation (λ = 1.540598 Å); bent Johann type [111] Ge-monochromator; 2θ/ω-scaning; 2θ-angle range is $4.000° \le 2\theta \le 120.000°$; detector's step is 0.480° (2θ); step scanned time is 250 s. The apparatus certification was carried out by standards NIST SRM 640b (Si), NIST SRM 676 ($Al_2O_3$) and NIST SRM ($LaB_6$).

The calculation of theoretical diagrams, X-ray profiles and phase analysis were carried out using of the program packet STOE WinXPOW (version 2.21) [29]. The refinement of crystalline structures of the phases by Rietveld method (Thompson- Cox-Hasting pseudo-Voigt function for approximation of X-ray reflexes) and for microstructure parameters calculation were performed by means of program FullProff.2k (version 4.0) [30] from the packet WinPLOTR [31].

The EPR spectra were investigated using Radiopan SE/X 2544 (Poland) and RE-1306 (Russia) radiospectrometers. The EPR signals were recorded at liquid nitrogen temperature in a special cryostat [27] made of sintered refined vitreous silica. Crystalline structure, phase composition and the microstructure parameters were stated at room temperature.

The XRD pattern of the ZnO powder is shown in Fig. 1. In accordance with the obtained experimental data and appropriate mathematical treatment the ZnO sample is a single-phase compound. The parameters of structure refinement and crystallography

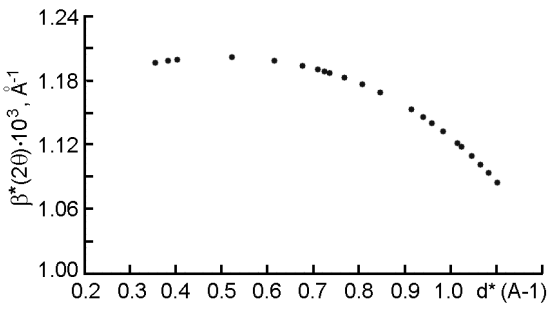


Fig. 2. Williamson-Hall plot for ZnO.

data are the following: the structure type is ZnO (zincite), Pearson symbol — hP4, $Z = 2$, space group — $P6_3mc$, lattice parameters — $a = 3.24985(1)$, $c = 5.20658(3)$ Å, $V = 47.622(1)$ Å$^3$. Atom coordinates of Zn in (2b) position: 1/3 2/3 0.0; isotropic thermal parameter is $B_{iso} = 0.400(15)$ (Å$^2$); the same for O atom in (2b) position: 1/3 2/3 0.3839(6); $B_{iso} = 0.31(7)$ (Å$^2$). The factors of reliability: $R_p = 0.0360$, $R_{wp} = 0.0138$, $R_F = 0.00957$; $\chi^2 = 3.93$.

The average size of particles is $<d> =$ 874.9(3) Å and average maximal stress is $<\varepsilon> = 0.041$ %. Fig. 2 illustrates the Williamson-Hall plot for a sample where the reciprocal peak widths $\beta^*(2\theta) = [\beta_0(2\theta)\cos\theta]/\lambda$ are plotted vs the reciprocal lattice distances $d^* = (2\sin\theta)/\lambda$, and $\beta_0$ is the line broadening. The resulting curve at small $d^*$ values fitted using $y(x) = c_1x + c_2$, where $c_1$ and $c_2$ are constants determining the $<\varepsilon>$ and $<d>$ values respectively. The deviation from the linear dependence $\beta^*(2\theta)$ is possibly caused by considerable contribution of the Gauss function to the description of the shape diffraction peaks.

The XRD pattern and refinement of crystalline structure of the $SiO_2$ powder are shown in Fig. 3. The examined sample is single-phase. The crystallography data and parameters of refinement are the following: the structure type is $SiO_2$ (α-quartz at room temperatures), Pearson symbol — hP9, $Z = 3$, space group – $P3_121$, lattice parameters – $a = 4.91296(3)$, $c = 5.40418(3)$ Å, $V = 112.966(1)$ Å$^3$. Si atom coordinates in (3a) position: 0.53056(21) 0 1/3; $B_{iso} = 0.49(2)$ (Å$^2$); the same for O atom in (6c) position: 0.4115(3) 0.1472(4) 0.1188(3); $B_{iso} = 0.86(4)$ (Å$^2$). The factors of reliability: $R_p = 0.0480$, $R_{wp} = 0.0650$, $R_B = 0.0325$, $R_F = 0.0382$; $\chi^2 = 4.24$.

The average size of $SiO_2$ particles is $<d> =$ 1095.4(1.1) Å and average maximal stress is

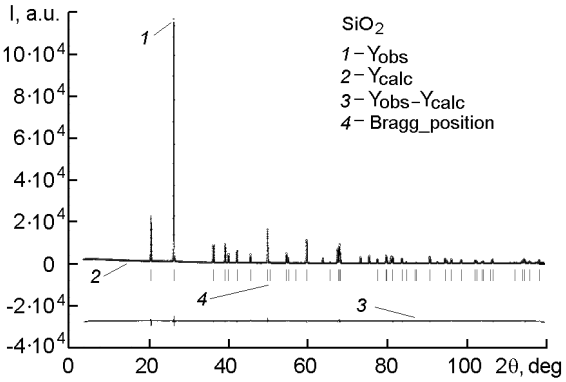


Fig. 3. X-ray diffraction data for $SiO_2$.

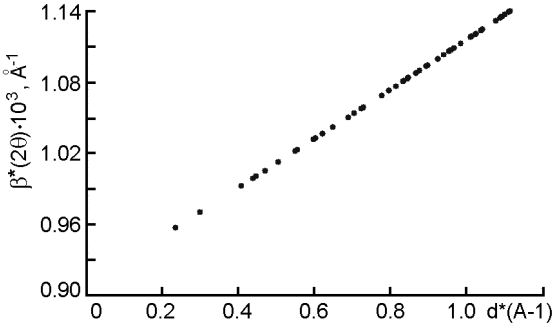


Fig. 4. Williamson-Hall plot for $SiO_2$.

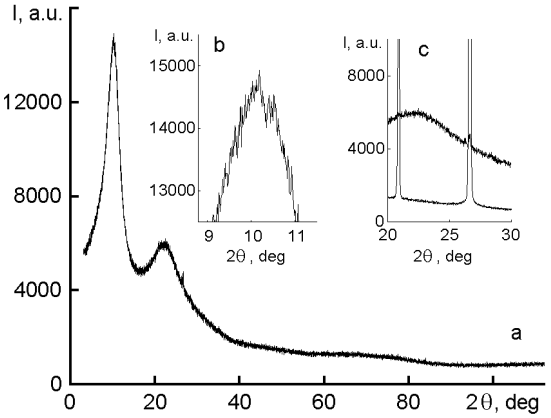


Fig. 5. XRD patterns of $SiO_2/10$ % $V_2O_5$ (a), and features in region of the first peak (b), and in region of α-quartz reflection [011] (c). In the insert (c) the top curve corresponds to sample $SiO_2/10$ % $V_2O_5$ and the below curve corresponds to crystalline $SiO_2$ as on Fig. 3.

$<\varepsilon>= 0.014$ %. As in the case ZnO the Fig. 4 shows the Williamson-Hall plot.

Experimental XRD pattern of the sample $SiO_2/10$ % $V_2O_5$ is given in Fig. 5a. The features of XRD spectra are shown on the inserts *b* and *c*. In the XRD pattern the three broad bands are observed at $2\theta \sim 10.1°$,

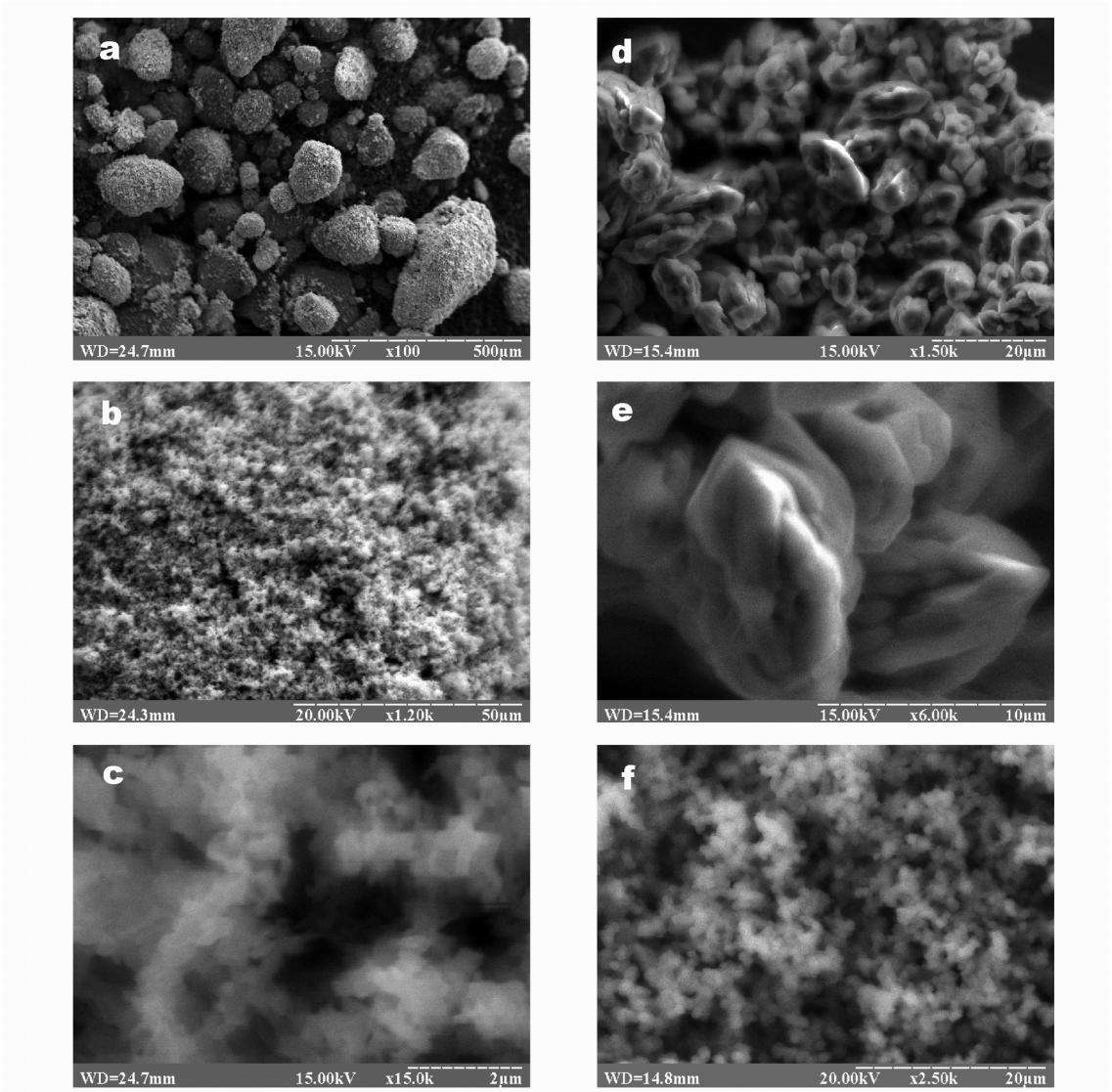


Fig. 6. SEM micrographs of the samples ZnO (a–c), $SiO_2$ (d, e), and $SiO_2$/10 % $V_2O_5$ (f) at different marker size.

22.5°, and 70.0°. The broad diffuse halos at 2θ ~ 22.5° and 70.0° are attributed to amorphous $SiO_2$. The same characteristic of broad peaks for the amorphous $SiO_2$ were observed previously [10, 11]. The maximal intensity reflection [011] (2θ = 26.6°) attributed to α-quartz and cause the additional peak (see insert *c*).

The first sharp double peak (2θ values are ~10.1° and ~10.5° respectively; see Insert b) of composite $SiO_2$/10 % $V_2O_5$, accounting for data [32, 33] on nanostructured $V_2O_5$, can be attributed to the 001 maximum reflection of $V_2O_5$. The observable peak 2θ ~ 10.1° is strongly broadened, obviously due to $V_2O_5$ nanodispersion in the composite. Thus, the nanocomposite $SiO_2$/10 % $V_2O_5$ contains the amorphous $SiO_2$, the additional phase of the crystalline α-quartz and the high-disperse $V_2O_5$.

The element X-ray microanalysis showed intense peaks of basic chemical elements and traces of noncontrolled impurities, such as Gd, Fe, Al, Ga, Mg, K. Due to the features of characteristic X-ray radiation [34], we can display the basic elements of nanopowders in our case. However, the identification of ion V (in nanocomposite) is complicated because of energetically closeness of the characteristic lines of ions O and V.

The typical micrographs of samples are presented on Fig. 6. SEM technique demonstrates the strongly sintered material. The dimensions of structural elements were

evaluated with the account of the authors' warning [28, 35] to the SEM technique. In nanocrystalline ZnO the large agglomerates with dimensions of 50–200 μm and with friable structure are observed. They consist of an ensemble of small particles with the dimensions ~0.08–0.10 μm. In $SiO_2$ nanocrystalline powder, formation of microobjects with dimensions ~6.2–12.5 μm is observed. In the synthesis conditions, the microstructures of a "rosette" type are formed, grouped by 3–5 particles and forming chains.

The morphology of nanocomposite $SiO_2/V_2O_5$ surface is illustrated by Fig. 6f. A polydisperse system is observable. The nearly spherical microobjects were obviously formed by conglutination of the individual starting nanoparticles. In the observation conditions, individual granules with a diameter near 0.36–4.00 μm are recorded. The relatively compact superaggregates with diameters of 0.60–0.80 μm are predominant. The latter form groups of a wide range of linear dimensions. In the case of $SiO_2$/(5–50 wt.%)$V_2O_5$ [26], the SEM micrographs are likely associated with the amorphous structure. At high temperature loading the sample seemed to organize in small (100 nm) spheroidal particles.

The measurements of the EPR spectra are performed at frequency $f = 9.156$ GHz and liquid nitrogen temperature. The information about quantity of the effective magnetic moment gives the spectroscopic splitting factor ($g$-factor). In general, $g$-factor depends on direction. We suppose as in the first approximation that there is the isotropic factor of the spectroscopic splitting ($g^*$-factor). The magnitude of $g^*$-factor is estimated in the frame of general formalism of the EPR method [36] for the one unpaired electron in strong magnetic field with induction $B$ as in the first approximation of single line in condition of resonance transition between two levels at frequency $f_0 = g^*\beta B_0/h$. Here β is the Bohr magneton,

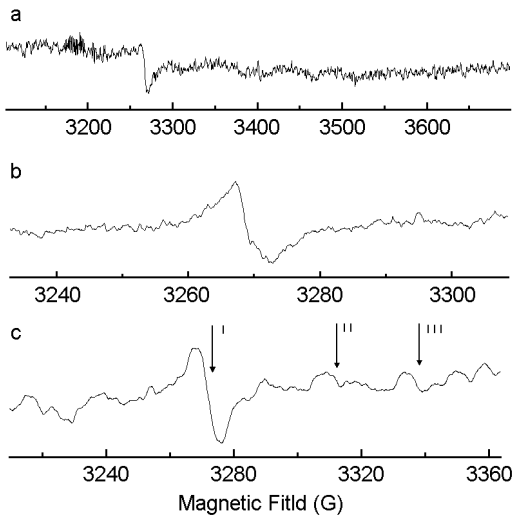


Fig. 7. The typical EPR spectra of samples $SiO_2$/10 %$V_2O_5$ (a, b), and ZnO (c) at 77 K. The curve (a) is general spectrum, (b) is dominate observed signal. On spectrum (c) the separate signals (I–III) are signed.

$B_0$ is external magnetic field, and $h$ is the Planck constant.

Experimental study of EPR signals of nanocomposite $SiO_2$/10 %$V_2O_5$ and ZnO were previously described in work [37]. In the case of $SiO_2$ nanopowder, no paramagnetic centres are detected. The Fig. 7 illustrates typical EPR lines of investigated nanopowders. Some parameters of the experimental observed EPR lines are given in the Table.

The EPR spectra were measured for samples just after preparation. Longer storage times of nanopowders led to weaker intensities of EPR signals.

In samples of $SiO_2/V_2O_5$ (Fig. 7 a–b) the EPR line with partial structure resolution are detected. The structure traces of measured line show high powder dispersion. Components of EPR signal (see Fig. 7b) are almost equidistant within the measurement accuracy. It is obvious that the structure is

Table. The parameters ($g^*$-factors and distance $\Delta B$ between limiting peaks of lines) of observe EPR-signals (correspondingly to Fig. 7). Numbers (I–III) are corresponded to EPR-signals sign on Fig. 7c.

| Number | Material | $g^*$-factor | $\Delta B$, mT |
|---|---|---|---|
| 1 | $SiO_2$–10 %$V_2O_5$ | 2.001±0.001 | 0.60±0.09 |
| 2 | ZnO | (I) 1.998±0.001<br>(II) 1.975±0.001<br>(III) 1.960±0.001 | 0.90±0.09 |

a result of splitting due to one unpaired electron coupling with nuclear spin of isotope $^{51}V$ (natural content is 99.75 %, spin of nucleus is **I** = 7/2 [18]). The estimate of the magnitude of splitting constant is $\alpha_0 = 0.19$ mT (defined as distance between components of structure). For interaction of one electron with one nucleus of $^{51}V$, $2\mathbf{I} + 1 = 8$ components of EPR spectrum are expected from calculations.

In the conditions of experiment the resolution of spectrum is insufficient. However, separation of the components of structure is complicated. The overlap of components is connected with possible broadening of lines (due to nanodispersion) and with the features of their intensity distribution [38]. At small anisotropy of *g*-factor in the system of chaotically oriented centres the intensities of lines are exactly characterized [18] by heterogeneous distribution. The intensities of the extreme lines with respect to the central line are inversely proportional to the distance between them (1/2 exponential law).

There are different views about the nature of EPR signals in nanocomposites $SiO_2/V_2O_5$. Thus, EPR signals were characterized by quite strong lines and associated by authors with paramagnetic $V^{4+}$-containing phases [24]. In [25], the EPR spectrum exhibits lines due to the hyperfine coupling of one unpaired electron with the $^{51}V$ nuclear spin in an axially distorted crystal field. Moreover, silica matrix practically does not affect the $V_2O_5$ structure and $V^{5+}$ centres were not reduced to $V^{4+}$, suggesting a weak interaction between the inorganic polymers (polyhedrons). The same EPR signals were detected in $V_2O_5$ xerogel. EPR revealed $V^{4+}$–O groups [26] in $VO_x/SiO_2$ catalysis pointing out normally from the compound surface and sitting in the centre of a surface array of oxygen atoms, suggesting that $g_{//} < g_{\perp}$ could be attributed to tetragonal distortion.

In accordance to obtained results [24, 26], the parameters (intensity, width) of EPR line and its hyperfine structure and the value of *g*-factor of EPR-signal in nanocomposite $SiO_2/V_2O_5$ strongly depend on preparation conditions.

The observable paramagnetic centre in $SiO_2/V_2O_5$ is formed in the nearest coordinating sphere of V ion. The structure of the measured EPR spectrum testifies about high-disperse form of the compound (see also XRD and SEM data) and interaction of unpaired electron with nucleus of vanadium ($^{51}V$). The $V^{5+}$ in EPR is not detected. In accordance with the data [24–26] the EPR spectra of the quinquivalent vanadium contained materials are connected with $V^{4+}$ ion. In this case unpaired electron interacts with nucleus of $^{51}V$.

As an alternative hypothesis we propose a probable link of the registered EPR-signal in $SiO_2/V_2O_5$ with an oxygen vacancy with one electron in its action field. The same electron presumably interacts with the $^{51}V$ nucleus. The vacancies as mentioned above are the basic point defects in nanopowders. The EPR signal in nanopowder $ZrO_2$ was ascribed [16] to the surface oxygen vacancy with a weak localized electron what is characterized by isotropic *g*-factor 2.003 and linewidth $\Delta B = 0.5$ mT.

Fig. 7c shows typical EPR spectra for ZnO nanopowder. Complex spectra with lines (I–III) are observed. The low intensity EPR-signals are registered in the lower and in the higher fields with respect to the central line. The EPR-signals with similar form and values of *g*-factors were detected at room temperature for nanopowder ZnO (the free surface is 3.6 $m^2/g$, p.a. Kemika, Zagreb) depending on external pressures up to 8 GPa [15]. At the same time in this ZnO nanopowder before pressing no EPR-signals were observed. For disperse ZnO under other conditions [15] paramagnetic centres were detected.

For pressure-compacted samples of ZnO, in accordance with EPR data analysis and comparison with the crystalline analog, values of *g*-factor of 1.96 to 2.02 are given [15]. The intensities of the six centres nonlinearly depended on pressure and temperature treatment. The dominant EPR signals were associated with the complex "double vacancy of Zn" and "vacancy of Zn".

Our measurements show that the major EPR signal (I) is most likely associated with single-charged oxygen vacancy ($g^* = 1.9976$, see the Table; the near values of *g*-factors $g\perp = 1.9965 \pm 0.0008$ and $g_{//} = 1.9950 \pm 0.0008$ were obtained by authors [15] in case of the same single vacancy). The intensities of the remaining observed lines (Fig. 7c) are small.

In [39], the EPR signal with the mentioned *g*-factor was ascribed to oxygen vacancy as well as to interstitial oxygen ion. We make preference to the first assumption since the interstitial oxygen ion exists in specially treated ZnO samples [28]. In [40], an oxygen vacancy with one unpaired electron coupled with isotope $^{67}Zn$ (natural containing is 4.11 %, spin of nucleus is **I** = 5/2)

was recorded by EPR method, as well as fine structure components. As in ref. [41], it was ascertained by EPR method that the donor-acceptor centres in powder ZnO were created in the presence of univalent impurities of alkali metals or intrinsic defects that are connected with deviation of stoichiometry.

Consequently the dominating signal (I) in the investigated ZnO can be connected with oxygen vacancies. The signals (II) and (III) (see Fig. 7c), as in [15, 40], are associated with shallow donor center and uncontrolled impurity (SEM data shows the presence of impurities) respectively. The low-intensity EPR signals are not identified as a result of low intensity (signal/noise ratio is nearly 1).

The nature of dominating paramagnetic centres is hypothetically ascribed to oxygen vacancy with one electron in its action field. As it is obvious from the performed experiments and from the analysis of literature data the establishment of nature of the paramagnetic centres is complicated what demands additional investigations. This problem is caused by complex composition and defect structure of nanodispersed systems, by the great function of surface states and by tendency to complexation in nanopowder ZnO as well as in nanocomposite $SiO_2/V_2O_5$.

Summing up, nanopowders ZnO, $SiO_2$, and composite $SiO_2/V_2O_5$ obtained by sol-gel technology have been investigated using XRD, SEM, and EPR methods as continuation of our measurements on pressed samples [42]. The obtained XRD and SEM results show satisfactory correlation with referenced structural data for corresponding compounds. The XRD pattern of the nanocomposite $SiO_2/10\ \%V_2O_5$ demonstrates the amorphous $SiO_2$, the additional phase of the crystalline α-quartz, and high-disperse $V_2O_5$. The $SiO_2$ and ZnO are single-phase nanopowders. The dimensions of nanograins obtained by XRD methods are smaller than the same dimensions obtained from SEM results. This is an evidence of aggregation of nanoparticles and formation of agglomerates of micro-dimensions.

## *References*


1. Medical Chemistry and Clinical Application of Silica, ed. by A.A.Chujko, Naukova Dumka, Kyiv (2003) [in Ukrainian].
2. A.L.Aseev, *Russian Nanotechnologies*, **1**, 97 (2006).
3. V.M.Hun'ko, I.F.Myronyuk, V.L.Chelyadyn et al., *Phys. and Chem. Solid State*, **8**, 321 (2007).
4. C.M.Mo, Y.H.Li, Y.Zhang, I.D.Zhang, *J.Appl. Phys.*, **83**, 4389 (1998).
5. B.K.Kotlyarchuk, I.F.Myronyuk, D.I.Popovych, A.S.Serednyts'kyj, *Phys. and Chem. Solid State*, **7**, 490 (2006).
6. P.P.Gorbyk, V.V.Levandovs'kyi, R.V.Mazurenko et al., *Phys. and Chem. Solid State*, **7**, 551 (2006).
7. V.G.Ponomareva, G.V.Lavrova, L.G.Simonova, *Sol. St. Ionics*, **119**, 295 (1999).
8. L.S.Semko, P.P.Gorbyk, L.P.Storozhuk et al., *Dopovidi NAN Ukrainy*, **3**, 153 (2007).
9. V.A.Zazhigalov, S.B.Grinenko, Yu.P.Zajtsev et al., *Nanosystemy, Nanomaterialy, Nanotechnolohii*, **2**, 215 (2004).
10. C.-B.Wang, R.G.Herman, C.Shi et al., *Appl. Catal. A:Gen.*, **247**, 321 (2003).
11. V.Murgia, E.M.F.Torres, J.C.Gottifredi, E.L.Sham, *Appl. Catal. A:Gen.*, **312**, 134 (2006).
12. V.I.Avdeev, G.M.Zhidomirov, *Zh. Strukt. Khim.*, **46**, 599 (2005).
13. R.A.Andrievskii, *Nanostrukturnoe Materialovedenie*, **1**, 5 (2005).
14. I.P.Suzdalev, Nanotechnology: Physics and Chemistry Nanoclasters, Nanostructures, and Nanomaterials, KomKniga, Moscow (2006) [in Russian].
15. M.G.Kakazey, G.N.Kakazey, J.G.Gonzales-Rodriguez, *Cryst. Res. Technology*, **36**, 429 (2001).
16. A.B.Bryk, M.D.Glinchuk, I.P.Bykov et al., *Nanostrukturnoe Materialovedenie*, **1**, 91 (2005).
17. A.B.Bryk, M.D.Glinchuk, I.P.Bykov et al., *Nanostrukturnoe Materialovedenie*, **1**, 67 (2006).
18. Ya.G.Klyava, EPR Spectroscopy of Disordered Solid State, Zinatne, Riga (1988) [in Russian].
19. A.Ye.Patracov, V.A.Gritsenko, G.M.Zhidomirov, *Fiz. Tverd. Tela*, **46**, 1955 (2004).
20. V.A.Gritsenko, Yu.N.Novikov, A.V.Shaposhnikov, Yu.N.Morokov, *Fiz. Tverd. Tela*, **35**, 1041 (2001).
21. A.V.Shaposhnikov, V.A.Gritsenko, G.M.Zhidomirov, M.Rodger, *Fiz. Tverd. Tela*, **44**, 985 (2002).
22. G.Sperlich, W.D.Laze, *Phys. Stat. Sol.(b)*, **65**, 625 (1974).
23. Yu.N.Belyaminov, V.S.Grunin, Z.N.Zonn et al., *Phys. Stat. Sol.(a)*, **27**, 165 (1975).
24. A.V.Kucherov, A.V.Ivanov, T.N.Kucherova et al., *Catal. Today*, **81**, 297 (2004).
25. G.N.Barbosa, C.A.Brunello, C.F.O.Graeff, H.P.Olivera, *J. Sol. State Chem.*, **177**, 960 (2004).
26. I.Rosetti, L.Fabbrini, N.Ballarini et al., *J. Catal.*, **256**, 45 (2008).
27. V.N.Shevchuk, D.I.Popovych, Yu.N.Usatenko et al., in: Regional Science Seminar Modern

Problems of Electronics, Lviv, Ivan Franko National University (2008), p.68.
28. A.V.Asadullaeva, S.B.Bazylev, V.M.Horyanoj et al., *Ukrainskii Metrolohichnyj Zh.*, **1**, 53 (2007).
29. Stoe WinXPOW, version 2.21, Stoe & Cie GmbH, Darmstadt, 2007.
30. J.Rodriges-Carvajl, *Commission on Powder Diffraction (IUCr). Newsletter*, **26**, 12 (2001).
31. T.Roisnel, J.Rodrigez-Carvajal, in: Materials Science Forum. Proc. Seventh European Powder Diffraction Conf. (EPDC 7), Barselona, Windows Tool for Powder Diffraction Patterns Analysis (2000), p.118.
32. D.C.Vin, M.Wang, W.D.Huang, *J. Mater. Sci. Lett.*, **18**, 1239 (1999).
33. A.Yu.Myshastyi, A.V.Shvetz, V.S.Dyadyun et al., *Zh. Fiz. Khim.*, **51**, 429 (2007).
34. V.D.Scott, G.Love, Quantitative Electron Probe Microanalysis, Ellis Harwoord Ltd, Chichester (1983).
35. Yu.D.Yagodkin, S.B.Dobatkin, *Zavodskaya Laboratoriya*, **73**, 38 (2007).
36. J.E.Wertz, J.R.Bolton, Electron Spin Resonance: Elementary Theory and Practical Applications, McGraw-Holl, New York (1974).
37. V.N.Shevchuk, Yu.N.Usatenko, D.I.Popovych, R.Ya.Serkiz, in: 5th Int. Workshop on Functional and Nanostructured Materials, Ivan Franko National University, Task Publishing Gdansk, Poland (2008), p.139.
38. S.A.Al'tshuler, B.M.Kozyrev, Electronic Paramagnetic Resonance of Interstitial Element Compounds, Nauka, Moscow (1972) [in Russian].
39. V.A.Nikitenko, *Zh. Prikl. Spect.*, **57**, 367 (1992).
40. J.M.Smith, W.E.Vehse, *Phys. Lett.*, **31A**, 147 (1970).
41. P.H.Kasai, *Phys. Rev.*, **130**, 989 (1963).
42. V.N.Shevchuk, D.I.Popovych, Yu.N.Usatenko et al., *Phys. and Chem. Solid State*, **10**, 289 (2009).

# Особливості структури та парамагнітні центри в оксидних нанопорошках

***В.Н.Шевчук, Д.І.Попович, Ю.М.Усатенко, П.Ю.Демченко, Р.Я.Серкіз***

Нанопорошки $ZnO$, $SiO_2$, $SiO_2/10\ \%V_2O_5$, отримані за sol-gel- технологією досліджено методом електронного парамагнітного резонансу (ЕПР) при температурі рідкого азоту. Структуру зразків проаналізовано з використанням методу рентгенівської дифракції. Морфологію поверхні та хімічний елементний склад порошків вивчено скануючим електронним мікроскопом. Для нанокомпозиту $SiO_2/10\ \%V_2O_5$ структура ЕПР спектра приписується результату взаємодії неспареного електрона з ядром ізотопу $^{51}V$. Домінуючий сигнал ЕПР у $ZnO$ попередньо пов'язується з однозарядною вакансією у кисневій підгратці.